

ORGANOMETALLICS

Volume 3, Number 7, July 1984

© Copyright 1984
American Chemical Society

Transition-Metal Carbides. A Comparison of Bonding in Extended and Molecular Interstitials

Sunil D. Wijeyesekera and Roald Hoffmann*

Department of Chemistry and Materials Science Center, Cornell University, Ithaca, New York 14853

Received August 31, 1983

The transition-metal "interstitial" carbides are interesting in that they have properties that are characteristic of their parent metal lattice as well as properties that result from strong metal-to-carbon bonds. In this paper we discuss this bonding by means of extended Hückel calculations on two common transition-metal monocarbide structures: the NaCl structure, found, for example, in NbC, and the WC structure. The preference for one or the other of these structures depends largely on the number of valence electrons per unit cell. There also exist a number of organometallic cluster carbides in which two common metal environments of carbon are the octahedron and the trigonal prism. Both the octahedral and the trigonal-prismatic clusters occur for well-defined electron counts, and one can compare them to the solid-state compounds where carbon is surrounded octahedrally (NaCl) or trigonal prismatically (WC) by metal atoms. Three questions we shall address are (i) the pervasiveness of the octahedron and the trigonal prism, (ii) the relevance of molecular-orbital calculations on the clusters for understanding the solids—what similarities and differences are there between the two, and (iii) an explanation of the differences in bonding that cause certain electron counts to favor a metal octahedron, and other electron counts to favor a metal trigonal prism. The discussion is extended to include other solid structures: NiAs, anti-NiAs, anti-CdI₂, and Fe₃C.

I. Introduction

What a wealth of information is hidden in the simple term "interstitial"! Let us consider an important example: the transition-metal carbides. Some properties of this class of compounds suggest that carbon atoms are just harmless interstitials filling in voids in the parent metal lattice. One example is the extremely wide range of carbon to metal ratios possible for many carbide structures. Another is the fact that like their parent metals they are good electrical conductors.¹

On the other hand, the interstitial atom has a marked effect on the structure and certain properties of the parent metal lattice. Rundle² first pointed out that transition-metal carbides of groups 4–6 never have the same metal lattice as their parent metal. Furthermore, starting with the WC structure (simple hexagonal lattice) and moving on to the extremely complicated carbides of Fe, Co, and Ni, this series exhibits structures that are unthinkable in a simple metal.

The property of carbides that most distinguishes them from their parent metals is their hardness. This hardness

is particularly marked among the monocarbides of groups 4–6. Over one million tons of WC is used annually in the U.S. in "cemented carbide" cutting tools.^{1a} One of the technological difficulties that had to be overcome is the brittleness of carbides at ordinary temperatures (WC is alloyed with cobalt to make it possible to work with it at lower temperatures). This brittleness is interesting to us in that it is generally considered to be a sign of *directed* bonding as opposed to the more isotropic bonding that is found in metals.

All this is to suggest that there are some interesting properties tied up in bonding to the interstitial atom. In order to investigate this bonding we performed band calculations using an extended Hückel³ tight binding method on a number of transition-metal carbides. There exist a number of good calculations in the literature on one of these structures, the NaCl structure of NbC.⁴ These have focused on the electrical properties, especially the very important high-temperature superconductivity of NbC and NbN. However, there has been very little quantitative discussion of bonding in these compounds and, in particular, no comparison of different structures.

(1) Three recent reviews on solid-state metal carbides are as follows: (a) Toth, L. E. "Transition Metal Carbides and Nitrides"; Academic Press: New York, 1971. (b) Kosolapova, T. Ya. "Carbides"; Plenum Press: New York, 1971. (c) Johansen, H. A. In "Survey of Progress in Chemistry"; Academic Press: New York, 1977; Vol. 8, pp 57–81.

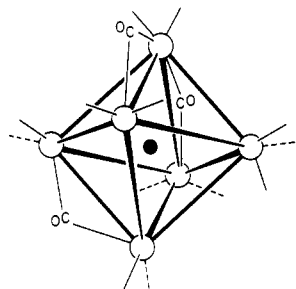
(2) Rundle, R. E. *Acta Crystallogr.* 1948, 1, 180–187.

(3) (a) Hoffmann, R. *J. Chem. Phys.* 1963, 39, 1397–1412. (b) Hoffmann, R.; Lipscomb, W. N. *Ibid.* 1962, 36, 2179–2189; 2189–2195.

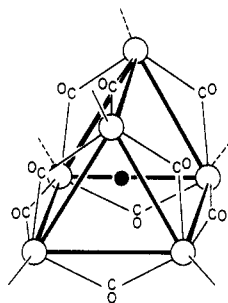
(4) Klein, B. M.; Papaconstantopoulos, D. A.; Boyer, L. L. *Phys. Rev. B.* 1980, 22, 1946–1966 and references therein.

II. Structure

We shall start by considering discrete molecules: the cluster carbides. A large number of such clusters have been made recently, extending in size up to fifteen metal atoms and two carbon atoms.^{5,6} Four and five metal atom clusters have exposed surfacelike carbon atoms and are considered in a separate paper.⁷ The smallest "bulklike" carbides have six metal atoms, which may be arranged either octahedrally or trigonal prismatically around a central carbon atom. Each of these clusters has a well-defined electron count. For instance, octahedral $\text{Ru}_6(\text{CO})_{16}\text{C}^{2-}$ (1) has four less electrons than trigonal-prismatic



● C ○ Ru



● C ○ Rh

2

$\text{Rh}_6(\text{CO})_{15}\text{C}^{2-}$ (2) (six electrons from the replacement of Ru by Rh minus two from one carbonyl ligand). A standard way of counting electrons is to count all valence electrons on the metal and carbide carbon atoms and to add two electrons per ligand. Hence, $\text{Ru}_6(\text{CO})_{16}\text{C}^{2-}$ has 86 electrons, and $\text{Rh}_6(\text{CO})_{15}\text{C}^{2-}$ has 90 electrons. A review by Muetterties⁵ lists nineteen 86-electron octahedral clusters and four 90-electron trigonal-prismatic clusters. The only exception is a Jahn-Teller distorted octahedron, $\text{Co}_6(\text{C-O})_{14}\text{C}^-$, which has 87 electrons.

Before discussing the structures of the solid-state carbides, we note the following interesting aspect of their nomenclature. Solid-state structures are often named after the first compound to have that type of structure. In general we will follow this convention. This means that we will refer to a group of carbides which have a structure

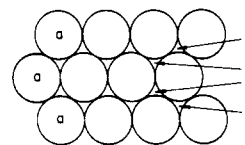
(5) For a recent review see: Tachikawa, M.; Muetterties, E. L. *Prog. Inorg. Chem.* 1981, 28, 203-238 and references therein.

(6) The following carbides and nitrides postdate ref 5 ("surface-like" carbide clusters are considered in a separate paper, ref 7): (a) Martinengo, S.; Gianfranco, C.; Sironi, A.; Heaton, B. T.; Mason, J. *J. Am. Chem. Soc.* 1979, 101, 7095-7097. (b) Albano, V. G.; Braga, D.; Martinengo, S. *J. Chem. Soc., Dalton Trans.* 1981, 717-720. (c) Albano, V. G.; Braga, D.; Ciani, G.; Martinengo, S. *J. Organomet. Chem.* 1981, 213, 293-301. (d) Bonfichi, R.; Ciani, G.; Sironi, A.; Martinengo, S. *J. Chem. Soc., Dalton Trans.* 1983, 253-256. (e) Blohm, M. L.; Fjare, D. E.; Gladfelter, W. L. *Inorg. Chem.* 1983, 22, 1004-1006. (f) Hayward, C.-M. T.; Shapley, J. R.; Churchill, M. R.; Bueno, C.; Rheingold, A. L. *J. Am. Chem. Soc.* 1982, 104, 7347-7349.

(7) Wijeyesekera, S. D.; Hoffmann, R.; Wilker, C. N., following paper in this issue.

isotypic with the NiAs structure as "the NiAs structure". The actual calculations will be on MoC. All of our calculations except for those on Fe_3C were done by using molybdenum and carbon parameters.

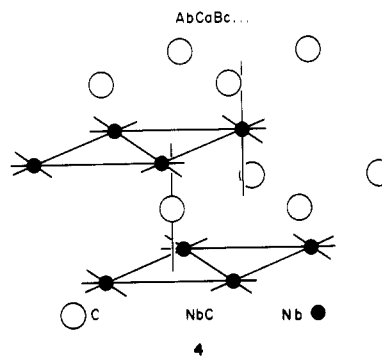
Our description of the solid-state carbides breaks them up into monocarbides (C:M ~ 1:1) and subcarbides. As mentioned earlier the monocarbides are among the hardest known solids, and hence are very important technologically. The two most common structures are those adopted by NbC and the α form of WC. They can be viewed as different ways of stacking hexagonal nets (3) one above



3

the other, such that an atom in the layer above lies above a threefold void in the lower layer. A single layer is completely specified by describing the (x, y) coordinates of a single atom. Hence, above a net with an atom centered at site a there are two equivalent threefold voids, b and c, only one of which must be filled to maintain the same unit cell. The reader will notice that we are using notation normally applied to fcc and hcp metals, except that alternate layers are now composed entirely of metal (A, B, or C) or carbon (a, b, or c).

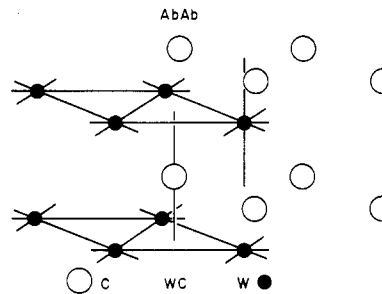
Structure 4 shows the NaCl structure of NbC with stacking sequence AbCaBc... In this arrangement, both metal and carbon atoms are octahedrally coordinated by atoms of the opposite type. The vertical axis is parallel



4

to the S_6 axis of the octahedra. There are twelve metal-to-metal contacts per metal atom, six in the plane, three above, and three below. In fact, the metal sublattice is just ACB... or fcc, and the whole structure consists of interpenetrating fcc lattices of niobium and carbon and is isomorphic to NaCl. The twelve carbon-to-carbon contacts per carbon atom are at the same distance as a metal-to-metal contact ($\sim 3 \text{ \AA}$) and could not possibly be a bond.

The alternate AbAb... structure is shown in 5. Now metal and carbon atoms are trigonal prismatically coordinated by atoms of the opposite type. There are eight



5

Table I. Distribution of the NaCl and WC Structure Types as a Function of the Number of Valence Electrons per Formula Unit^a

structure type	no. of valence electrons				
	8	9	10	11	12
NaCl	TiC ZrC HfC	VC NbC TaC	VN MoC _{1-x} WC _{1-x}	CrN	
WC			MoC WC TaN	MoN WN	(RuC?) (OsC?)

^a Toth also lists a number of ternary nitrides with the WC structure ranging from Ti_{0.7}Co_{0.3}N (10.5 electrons) to Mo_{0.8}Ni_{0.2}N_{0.9} (11.3 electrons).

metal-to-metal contacts per metal atom; in fact the metal sublattice is simple hexagonal. This is the WC structure.

These structures represent extremes among an infinite range of possibilities. If the metal is octahedrally coordinated by carbon but carbon is trigonal prismatic coordinated by the metal, we have the *NiAs* structure. The reverse structure, known as *anti-NiAs*, has the stacking sequence AbCbAbC... and is found for one phase of NbN.^{1a}

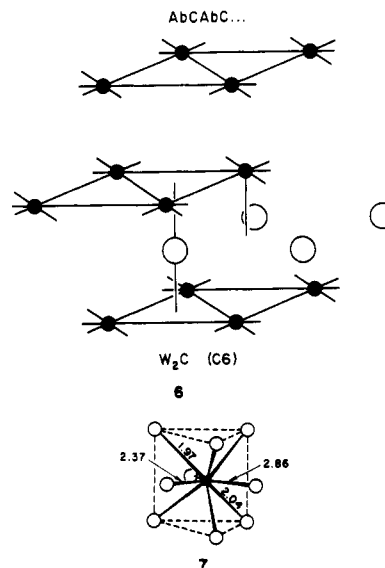
Unlike the discrete carbides, the NaCl and WC structure types are not characterized by a single electron count. However, the occurrence of a given structure can still be correlated to the electron count. In Table I⁸ the carbides are arranged according to the number of valence electrons per formula unit.

For nine or less valence electrons per formula unit, only the NaCl structure is found. For 10 or more valence electrons, the WC structure is more common, and many of the exceptions are not really contradictory. For instance, although WC shows both the WC and NaCl structures, the latter is only found when there are defects in the carbon lattice. Then there is less than one carbon atom per formula unit and hence less than 10 electrons per formula unit.

Monocarbides of the late transition metals are not found or are extremely unstable. Hence, although RuC and OsC have been reported as having the WC structure, this result was not reproducible.^{1b} ReC and TcC have also been suggested, but their structure is not known.

A considerable amount of carbon can be removed from a monocarbide without changing the metal lattice. Eventually, however, the metal lattice changes, the carbon vacancies order, and we have one of the subcarbides. In subcarbides of the early transition metals, the metal lattice is still close packed but not necessarily cubic close packed.⁹ We shall consider one such structure, 6, the anti-CdI₂ or C6 structure¹⁰ adopted by the α form of Ta₂C and W₂C. This structure may be derived by removing alternate layers of carbon from the carbide with an anti-NiAs structure. Hence, the metal lattice is hexagonal close packed.

The late 3d transition metals form subcarbides that are based on a very complex metal lattice. It is easiest to focus on the local environment of carbon, which is in many cases a tricapped trigonal prism.¹¹ The local environment of carbon in Fe₃C cementite is shown in 7.¹² Other examples

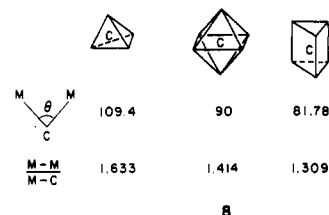


of the tricapped trigonal prism are Fe₅C₂, Mn₇C₃,¹³ and Cr₃C₂.¹⁴ Two or three of these structures are found for each of the carbides from Cr-Co; hence the structures do not sort easily by electron count. Although the tricapped trigonal prism is not known for discrete metal clusters, there are now two examples where two of the rectangular faces of a trigonal prism are capped.¹⁵ As in cementite, the metal-to-carbon distances to the capped faces are much longer than the metal-to-carbon distances within the trigonal prism.

III. General Approach

The rest of this paper will follow the following general line. (i) The octahedral cluster will be used to help us understand bonding in the NaCl structure of NbC. (ii) The trigonal-prismatic cluster will be compared to the octahedral cluster, and the WC structure will be compared to the NaCl structure of NbC. (iii) We will generalize to consider some of the other solid-state structures just described.

But first we must ask the question: why is the metal surrounding the carbon atom either octahedral or trigonal prismatic? After all, isn't carbon quadrivalent? In 8 are



shown the ideal M-M/M-C ratios for a tetrahedron, octahedron, and regular trigonal prism. We may also calculate this ratio for a given metal by considering the metal-to-metal distance in the bulk metal, and the metal-to-carbon distance in the carbide. The result is 1.38 for hafnium, one of the largest transition metals, and 1.23 for

(8) Most entries in Table I come from ref 1a. The exception is TaN₁₀ (WC structure) from Brauer et al. (Brauer, G.; Mohr-Rosenbaum, E. *Monatsh. Chem.* 102, 1311-1316.)

(9) For a review and notation for these subcarbides see: Parthe, E.; Yvon, K. *Acta Crystallogr., Sec. B* 1970, B26, 153-163.

(10) Strukturbericht symbols such as C6 are an alternate way of naming structure types. A complete list is given in: Pearson, W. B. "A Handbook of Lattice Spacings and Structures of Metals and Alloys"; Pergamon Press: Oxford, 1958; Vol. I.

(11) Other arrangements of transition-metal atoms around a carbon atom are a square antiprism (Cr₂₃C₂) and an octahedron (Ni₃C, Co₂C).

(12) (a) Fasiska, E. J.; Jeffrey, G. A. *Acta Crystallogr.* 1965, 19, 463-471. (b) Senateur, J.-P. *Ann. Chim. (Paris)* 1967, 103-122.

(13) For a nice discussion of tricapped trigonal-prismatic phases adopted by carbides and borides see: Aronsson, B.; Rundqvist, S. *Acta Crystallogr.* 1962, 15, 878-887.

(14) Meinhart, V. D.; Krisement, O. *Z. Naturforsch. A* 1960, 15A, 880-889.

(15) (a) Albano, V. G.; Braga, D.; Chini, P.; Martinengo, S. *J. Chem. Soc., Dalton Trans.* 1982, 645-649. (b) Albano, V. G.; Braga, D.; Chini, P.; Strumolo, D.; Martinengo, S. *Ibid.* 1983, 249-252.

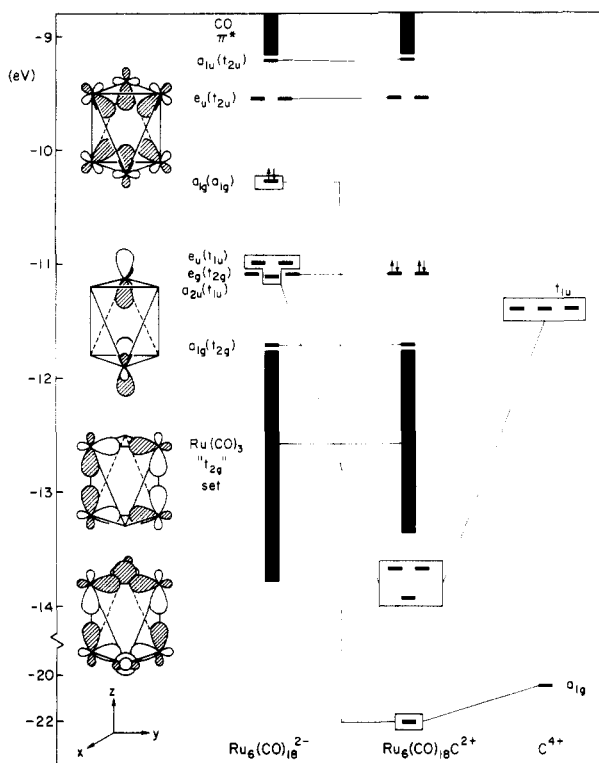


Figure 1. Interaction diagram for the formation of $\text{Ru}_6(\text{CO})_{18}\text{C}^{2+}$ from $\text{Ru}_6(\text{CO})_{18}^{2-}$ and C^{4+} . The metal framework is octahedral. The boxed frontier orbitals drawn interact with carbon s, p_x , p_y , and p_z (top to bottom).

iron, one of the smallest transition metals. These ratios are clearly a better fit to the results for the octahedron and trigonal prism than for the tetrahedron. This means that if we were to have a tetrahedral arrangement of metal atoms around carbon, the polyhedra would be so stretched that metal-to-metal bonds would have to be broken. Ipso facto, the absence of tetrahedral carbides implies that metal-to-metal bonding is important in stabilizing the carbide.

IV. Metal Octahedra

The experimental fact is that, according to the counting scheme described earlier, octahedral six-metal clusters have 86 electrons. This is true whether or not carbon or another interstitial is present, provided we count the valence electrons of the interstitial. This 86 electron count has been explained in two ways: first, by a qualitative analogy to the boron hydrides, the Wade-Mingos rules;¹⁶ second, by quantitatively considering the bare metal cluster. The calculations of Mingos¹⁷ and Lauher¹⁸ are important here.

We have chosen to consider the idealized cluster $\text{Ru}_6(\text{CO})_{18}\text{C}^{2+}$. This makes use of the isolobal analogy between $\text{Ru}(\text{CO})_3$ and BH, the basis of the Wade-Mingos rules. Real octahedral clusters contain 15–17 ligands; since the 86-electron rule works both for 18 ligands and for no ligands, the extra electrons must be tied up in nonbonding orbitals.

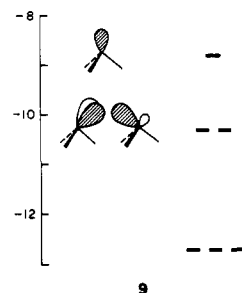
(16) (a) Wade, K. *Chem. Commun.* **1971**, 792–793. (b) Wade, K. *Inorg. Nucl. Chem. Lett.* **1972**, *8*, 559–562. (c) Wade, K. "Electron Deficient Compounds"; Nelson: London, 1971. (d) Mingos, D. M. P. *Nature (London) Phys. Sci.* **1972**, *236*, 99–102.

(17) (a) Mingos, D. M. P. *J. Chem. Soc., Dalton Trans.* **1974**, 133–138. (b) Mingos, D. M. P.; Forsyth, M. I. *Ibid.* **1977**, 610–616; **1976**, 1163–1169. (c) Mason, R.; Thomas, K. M.; Mingos, D. M. P. *J. Am. Chem. Soc.* **1973**, *95*, 3802–3804.

(18) Lauher, J. W. *J. Am. Chem. Soc.* **1978**, *100*, 5305–5315; **1979**, *101*, 2604–2607.

Figure 1 shows an interaction diagram for the formation of the carbide from $\text{Ru}_6(\text{CO})_{18}$ and carbon. The orbitals are labeled both according to their pseudooctahedral symmetry, the symmetry of the Ru_6 skeleton, and their actual D_{3d} symmetry, the symmetry of the molecule. Other details of the geometry are included in the Appendix.

The orbitals on the left-hand side of Figure 1 divide up approximately according to their parentage in the $\text{Ru}(\text{CO})_3$ fragment, the level diagram for which is shown in 9. The



σ - and π -type frontier orbitals have been described in previous papers.¹⁹ The interaction of six $\text{Ru}(\text{CO})_3$ fragments should give rise to 18 orbitals; the symmetries of which are identical with $\text{B}_6\text{H}_6^{2-}$:²⁰

$$\sigma: a_{1g}, t_{1u}, e_g$$

$$\pi: t_{1u}, t_{2g}, t_{2u}, t_{1g}$$

where σ -type fragment orbitals point toward the center of the octahedron, and π -type fragment orbitals are tangential to the center of the octahedron.

$\text{B}_6\text{H}_6^{2-}$ has seven bonding orbitals of symmetry a_{1g} , t_{1u} and t_{2g} ; the analogous orbitals of $\text{Ru}_6(\text{CO})_{18}$ are seen in Figure 1. Only three of the eleven antibonding orbitals are shown in this figure; the others are lost in the block of $\text{CO } \pi^*$. The orbitals of $\text{Ru}_6(\text{CO})_{18}$ which interact best with carbon are also shown in this figure. Bonding with carbon is accomplished by orbitals of a_{1g} symmetry (carbon s) and t_{1u} symmetry (carbon p). There is only one a_{1g} orbital derived from the frontier set of $\text{Ru}(\text{CO})_3$, and it is occupied. On the other hand, there are two t_{1u} sets, one occupied and one unoccupied. These are derived from both π -type and σ -type $\text{Ru}(\text{CO})_3$ frontier orbitals; the occupied set is mostly π whereas the unoccupied set is mostly σ . This is because the t_{1u} combination of σ FMO's is metal-to-metal nonbonding. Also the π FMO is lower in energy than the σ FMO, 9.

As Figure 1 shows, the major interaction of carbon p is with the occupied t_{1u} set. This is a crucial point, as it implies that no new occupied orbitals are introduced on interaction of $\text{Ru}_6(\text{CO})_{18}$ with carbon, and that the 86-electron rule must still hold. An obvious reason that the occupied t_{1u} set interacts better is a better energy match. Furthermore the size of the overlap of the σ FMO on $\text{Ru}(\text{CO})_3$ with carbon is about the same as the size of the π overlap. This surprising fact is easily explained: The so-called σ FMO is strongly delocalized by interaction with $\text{CO } \pi^*$ so that it is only 30% on the metal. There is another σ orbital, which is 70% on the metal, but it is much higher in energy.

The principal result of the interaction of the frontier orbitals of $\text{Ru}_6(\text{CO})_{18}$ with carbon p orbitals is a set of three orbitals lying just below the fragment t_{2g} set. The fact that

(19) Albright, T. A.; Hoffmann, P.; Hoffmann, R. *J. Am. Chem. Soc.* **1977**, *99*, 7546–7557.

(20) (a) Eberhardt, W. H.; Crawford, B. L., Jr.; Lipscomb, W. N. *J. Chem. Phys.* **1954**, *22*, 989–1001. (b) Longuet-Higgins, H. C.; Roberts, M. deV. *Proc. R. Soc. London, Ser. A* **1954**, *A224*, 336–347.

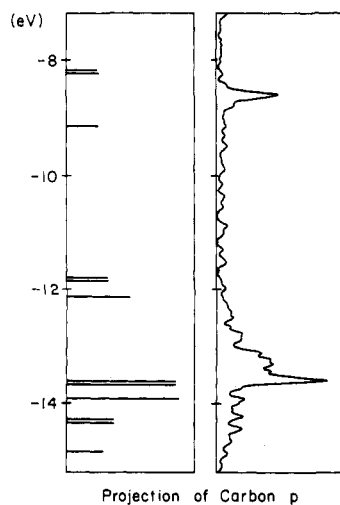


Figure 2. Projection of carbon p orbitals as described in the text. On the left is the octahedral cluster; on the right is the solid with the NaCl structure of NbC.

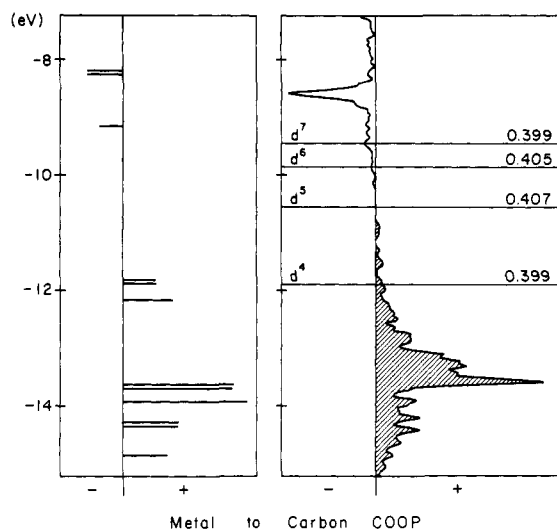


Figure 3. Metal-to-carbon crystal orbital overlap population (COOP): left, cluster; right, solid. The numbers on the solid-state curves are the integrated overlap populations for the Fermi levels indicated. It is clear from the relative sizes of the bonding and antibonding components that most antibonding orbitals are off-scale.

these orbitals are lower in energy than the metal-to-metal bonding orbitals reflects the greater strength of metal-to-carbon bonding. The principal result of the interaction of the frontier a_{1g} orbital of $Ru_6(CO)_{18}$ with the carbon s orbital is an orbital lying very low in energy (~ 22 eV). It is worth noting that this interaction is sizable in spite of a large energy difference between the two orbitals involved. These two a_{1g} orbitals have a very large overlap.

Unfortunately, in our delocalized molecular-orbital picture it is not possible to trace all the metal-to-carbon bonding to a single orbital, especially for a large cluster containing 42 atoms. A better picture of the bonding of carbon p orbitals is given in Figures 2 and 3. In the left side of Figure 2 all orbitals which were more than 5% carbon have been plotted; the length of the line drawn for an orbital is proportional to the percentage of carbon in the orbital. We see the three orbitals previously referred to lying just above 14 eV; these are the longest lines. We also see three orbitals at the top of the fragment t_{2g} set, as well as some others deeper down. The top three orbitals shown are empty, and we suspect metal-to-carbon antibonding. In Figure 3 at left we shown the same orbitals, now weighted by their contribution to the metal-to-carbon

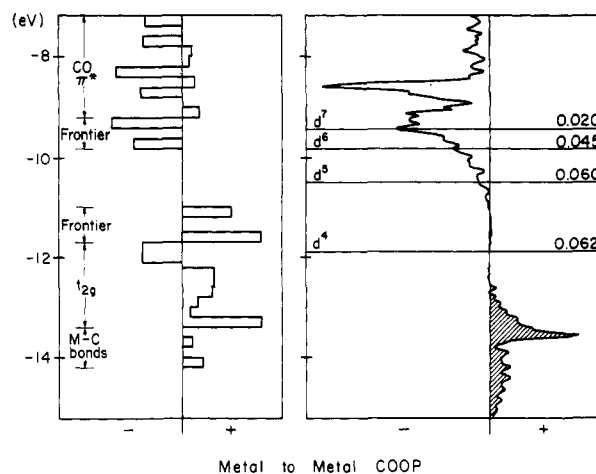


Figure 4. Metal-to-metal COOP: left—cluster; right—solid. The difference between the two curves lies in the occupation of antibonding " t_{2g} " orbitals in the cluster.

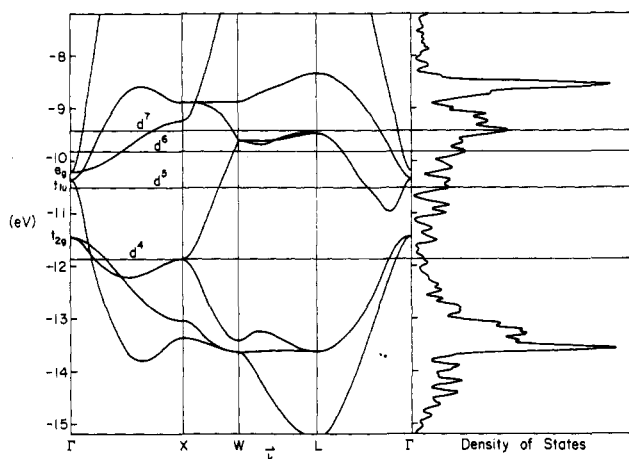


Figure 5. Band structure (left) and density of states (right) for the solid with the NaCl structure (NbC). The wide bands and absence of a band gap are typical of a metal.

overlap population. The interpretation of this figure is simple: orbitals to the right of the base line (+) are metal-to-carbon bonding; orbitals to the left of the baseline (-) are metal-to-carbon antibonding.

If we try to use a similar plot to describe metal-to-metal bonding, we run into difficulties, since there are many orbitals involved in metal-to-metal bonding. Instead, in Figure 4 at left we have constructed a histogram of step size 0.2 eV. All orbitals within a step are weighted according to their contribution to the metal-to-metal overlap population, and the weights are added up.

In order to interpret Figure 4 more easily we divided up the energy range according to the notation used in Figure 1. The lowest orbitals shown are the metal-to-carbon bonds which are seen to also be metal-to-metal bonding. Next is the fragment t_{2g} set; the lower end of which is bonding, the upper end antibonding. Above the t_{2g} set lie the bonding frontier orbitals, a HOMO-LUMO gap, and the antibonding frontier orbitals. Finally, we have the band labeled $CO \pi^*$, within which are buried metal-to-metal antibonding frontier orbitals.

To sum up, Figures 2-4 are useful pictorially in showing the bonding in situations where many orbitals are involved. They prepare us for applying similar methods of analysis to the solid state, where the number of orbitals is infinite. We performed calculations on the NaCl structure of NbC using the parameters for Mo and C given in the Appendix. The distance molybdenum-carbon was 2.1845 Å; molybdenum-molybdenum was 3.09 Å.

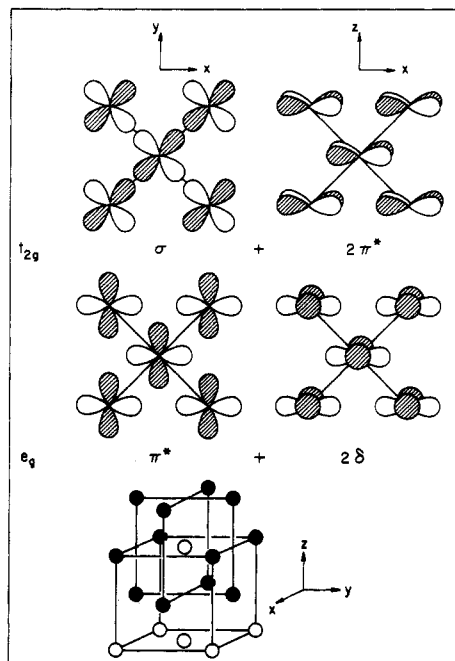


Figure 6. The metal d orbitals at $k = (0, 0, 0)$, the Γ point. Nearest-neighbor metal atoms are shown in the plane of the orbital (left) and in one of the two planes perpendicular to the orbital (right).

The two ways of describing the orbitals of a solid are shown in Figure 5. One is to plot the energies for a subset of k points and hence a subset of orbitals. These are the high-symmetry lines. This band structure is depicted on the left of Figure 5. The energy range covered starts with the d band of the metal and the p band of carbon, i.e., carbon s is off-scale in the range -20 to -25 eV.

Since the orbitals have high symmetry they are relatively easy to interpret. Let us consider the Γ point, at which the phases of the orbitals in different unit cells are the same. The point symmetry of these orbitals is the same as the point symmetry of the solid, O_h . Carbon p orbitals have t_{1u} symmetry and hence mix only with metal p orbitals. The metal d orbitals, t_{2g} and e_g , are split solely due to metal-to-metal interaction. This is shown in Figure 6, where we have returned to a conventional view of the unit cell of NbC, which is isostructural with NaCl. The 12 metal nearest neighbors of a metal atom lie in three mutually perpendicular planes, as shown. The six carbon neighbors of a metal atom are not shown, they lie along the x , y , and z axes. t_{2g} orbitals point between carbon neighbors but toward four metal atoms, those in the plane of the orbital. e_g orbitals point toward nearest neighbor carbon atoms and avoid metal atoms. We have shown one t_{2g} orbital (xy) and one e_g orbital ($x^2 - y^2$), both in the plane of the orbital and in one of the two planes perpendicular to the plane of the orbital. Interactions in the plane of the orbital dominate; the net effect is that t_{2g} is bonding, e_g antibonding; the splitting is 1.2 eV.

Since metal d orbitals at the Γ point do not interact with carbon p, their energies are a good indication of the relative H_{ii} 's for metal d and carbon p. The very accurate calculations of Klein⁴ et al. on NbC indicate a t_{2g} - e_g splitting of ~ 2 eV and a carbon orbital which lies 0.4 eV above the t_{2g} set. Hence our relative H_{ii} 's for molybdenum vs. carbon differ from his results for niobium vs. carbon by 1 eV. Molybdenum lies lower in energy than niobium, in agreement with electronegativity arguments.

It is clear that the Γ point is not representative of the solid, since it does not contain bonding between metal d and carbon p. The unrepresentative nature of high-sym-

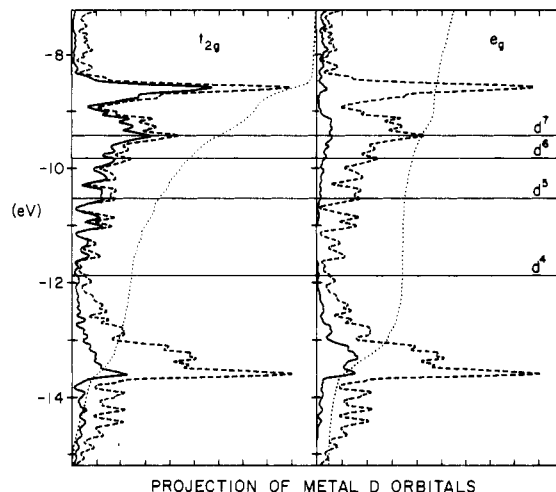


Figure 7. Projection (solid curves) of metal t_{2g} and e_g orbitals for MoC (NaCl). The total DOS (dashed) is provided for reference. The dotted curve is the integral of the projection on a scale of 0-100% full.

metry points is a generic problem with metals, in which there are wide bands and hence sharp changes in orbital character between k points. The solution is to consider all of the orbitals, expressed in the form of a density of states. In practice, this was done by considering a finite number of k points (108) scattered throughout the Brillouin zone (a special points set). A histogram was constructed (step size $1/30$ eV) similar to that found in Figure 4 except that each state is equally weighted. Finally, a Gaussian of half-width 0.1 eV was used to smooth the data. This density of states is shown at the right in Figure 5.

In addition, to aid in interpretation, we constructed density-of-states histograms in which each state was weighted by metal t_{2g} or e_g character (Figure 7), carbon p character, metal-to-carbon overlap population, and metal-to-metal overlap population (right-hand side of Figures 2-4). The first three are referred to simply as projections of the various orbitals and actually contain three curves each. The projection (solid) is compared to the total density of states (dashed). The dotted curve is the integral of the projection constructed such that the base line corresponds to no filling of the orbital and the right-hand margin to 100% filling of the orbital. The overlap population weighted curves have been given the name COOP (crystal orbital overlap population) and are a very nice indicator of whether electrons added to a given system go into bonding (+) or antibonding (-) orbitals. The bonding regions of the COOP curves have been shaded.

V. A Comparison of the Solid with the Cluster

Our solid-state results are made clearer by a comparison with the cluster.

In both cases metal-to-carbon bonding is strong, and the metal-to-carbon bonding orbitals are pulled down deep, away from the Fermi level and into the range 13-14 eV (Figure 2). In the cluster, bonding to the carbon atoms as well as to the carbonyl ligands is accomplished through metal $d^2 sp^3$ hybrids. This means that only two of the fragment d orbitals, the e_g set, are involved. Since the local environment of a metal atom in the solid-state compound is six carbon atoms arranged in an octahedron, ligand field arguments indicate that again only the e_g set of metal orbitals is involved in bonding to carbon.

The integrated projection of e_g orbitals in MoC (NaCl structure) (Figure 7) shows this clearly. Five percent of these orbitals are already occupied at -15.2 eV; this portion of the e_g set must be bonded to carbon s. The most distinct

change in occupation of these orbitals occurs between -13 and -13.75 eV; the metal-to-carbon p bonding orbitals in Figure 3 are also found in this energy range. Finally, 45% of this orbital is still unoccupied at -7.2 eV, just as most of the metal-to-carbon antibonding orbitals lie above this energy. In short, occupation of the e_g orbitals follows metal-to-carbon bonding projections.

Those orbitals on the metal atom which are not involved in bonding to carbon spread out into a band due to metal-to-metal interaction. In the cluster, there is a set of occupied metal-to-metal bonding orbitals separated from a set of unoccupied metal-to-metal antibonding orbitals by a HOMO-LUMO gap. In the solid state there is an infinite set of combinations of metal orbitals and hence no band gap; the carbide is a metal. The solid-state equivalent of the HOMO-LUMO gap is a dip in the density of states, corresponding to a region of approximately nonbonding orbitals between a bonding and an antibonding region (see Figure 4). Not unexpectedly, many of the experimentally known compounds have their Fermi level inside this dip.

Since kT at room temperature (0.02 eV) is very small on the scale of our density of states, certain properties of a solid which are related to thermal excitation of electrons are proportional to the density of states at the Fermi level.²¹ By examining these properties for the known d^4 and d^5 compounds, we can verify that the density of states is indeed low for these electron counts. One such property is the electronic specific heat coefficient,²² which is very low, especially for d^4 carbides but also for d^5 carbides and d^5 nitrides. Magnetic susceptibility²³ measurements support this conclusion. They also indicate that the density of states increases rapidly on removing carbon, and hence electrons, from d^4 carbides. A similar rigid-band interpretation of microhardness²⁴ in TaC_{1-x} implies that antibonding orbitals are first occupied between d^4 and d^5 .

In the preceding discussion, we turned on interactions in the order metal-to-carbon followed by metal-to-metal. It is also instructive to turn on metal-to-metal interactions first. This is what is done explicitly in Figure 1, if we ignore the field of the carbonyl ligands. Let us concentrate only on those orbitals derived from the frontier orbitals of $Ru(CO)_3$. The metal orbitals first spread into a band; there is a small gap between filled and unfilled orbitals. Carbon interacts mainly with the bottom of the band (filled orbitals), and the main effect is to widen considerably the HOMO-LUMO gap. Finally, we note that not all of the metal-to-metal bonding combinations of $d^2 sp^3$ hybrids interact with carbon. The "band gap" in the carbide occurs between these remaining bonding orbitals and the unperturbed antibonding set.

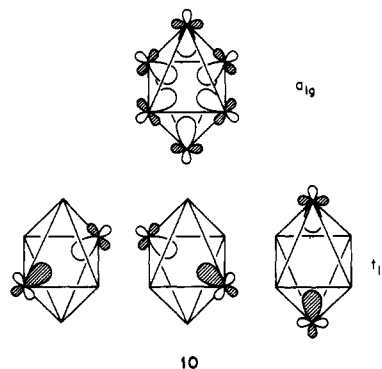
MoC (NaCl structure) actually behaves slightly differently from the above description, and the reason is the different environment around the metal. If we were to derive a cluster to represent the environment around carbon in a solid, we would come up with six MC_5 frag-

Table II. Overlap Populations (Metal-Metal and Metal-Carbon) for the Octahedral Cluster and Solid

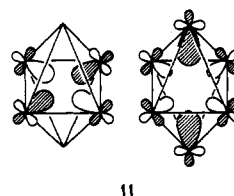
molecule	overlap population	
	M-M	M-C
$Ru_6(CO)_{18}^{2-}$	0.206	
$Ru_6(CO)_{18}C^{2+}$	0.119	0.408
$Mo(fcc)$	0.231	
$MoC(NaCl)$	0.060	0.407

ments around a central carbon atom. Then, once we turn on all interactions, the metal would have the correct ligand field.

Again we concentrate on the frontier orbitals of ML_5 ; this fragment differs from an ML_3 fragment in having only one, σ -type, frontier orbital. Four of the six symmetry-adapted linear combinations of this frontier orbital, those of symmetry a_{1g} and t_{1u} , interact with carbon. These



four orbitals are either metal-to-metal bonding or metal-to-metal nonbonding. Hence, as in the cluster, carbon interacts with the bottom of the band formed by metal-to-metal interaction. The other two linear combinations, 11, have symmetry e_g which matches a d orbital. Hence, these metal-to-metal antibonding orbitals cannot interact with carbon.



We can now understand in broad terms the difference between the clusters and the extended solids. In Figure 8 (top), we show in a schematic diagram the construction of the cluster levels. An ML_3 fragment is hexamerized, creating a t_{2g} band and some framework levels. Some of these are M-M bonding, some nonbonding, and some antibonding. The carbon atom interacts with some of the framework levels to give a set of M-C bonding orbitals and a corresponding antibonding set. In the composite cluster carbide all M-C and M-M bonding levels are filled, and this occurs for electron counts greater than d^6 , around d^8 .

Contrast the extended carbide. The metal orbitals interact strongly with each other, creating a relatively wide d band, and some framework orbitals, four of which point toward the cavity to be occupied by the carbon. The carbon interacts with these orbitals to give M-C bonding and antibonding combinations. If M-C and M-M bonding is to be maximized, only the bottom of the t_{2g} band can be filled, for the top is M-M antibonding. Only low d electron counts allow this, and high counts, such as those observed for the discrete clusters, would be disruptive of all bonding.

(21) Ashcroft, N. W.; Mermin, N. D. "Solid State Physics"; Holt, Rinehart and Winston: New York, 1976; pp 47-49 (specific heat), p 663 (magnetic susceptibility).

(22) Reference 1a, p 199.

(23) (a) Reference 1a, p 195. (b) Bittner, H.; Goretzki, H. *Monatsh. Chem.* 1960, 91, 616-619; 1962, 93, 1000-1004. (c) Bittner, H.; Goretzki, H.; Benesovsky, F.; Nowotny, H. *Ibid.* 1963, 94, 518-526. (d) Ishikawa, M.; Toth, L. E. *Ibid.* 1972, 103, 492-502. (e) Borukhovich, L. B.; Dubroskaya, B.; Matveenko, I. I.; Geld, P. V. *Phys. Status Solidi* 1969, 36, 97-102.

(24) (a) Santoro, G. *Trans. Metall. Soc. AIME* 1963, 227, 1361-1368. (b) Steinitz, R. In "Nuclear Applications of Nonfissionable Ceramics"; Boltax, A., Handwerk, J. M., Eds.; American Nuclear Society: Hinsdale, IL, 1966; p 50. (c) Rowcliffe, D. J.; Warren, W. J. *J. Mater. Sci.* 1970, 5, 345-350.

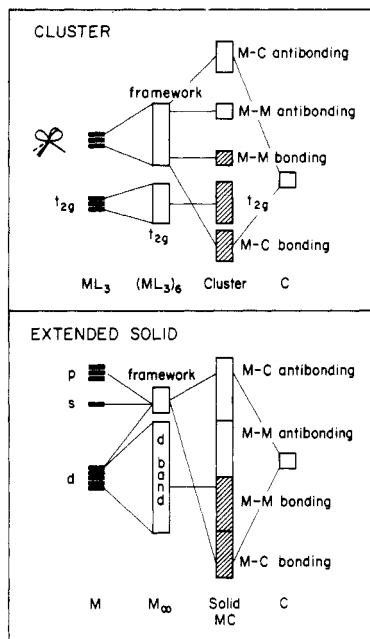


Figure 8. A schematic diagram of bonding in a discrete cluster and an extended carbide, explaining why the former allows *d* electron counts much greater than the latter. See text for discussion.

Otherwise, every aspect of the interaction with carbon in Figure 1 has its analogy in the solid-state compound. For example, carbon increased the HOMO-LUMO gap in the cluster. We recall that the equivalent of the gap in the cluster is a dip in the density of states between bonding and antibonding orbitals in the solid. Both experiment²⁵ and theory indicate that this dip is neither as deep nor as broad in the transition metal as it is in the carbide.

The final analogy concerns the effect of added carbon on metal-to-metal bonding, as measured by the overlap population. The appropriate overlap populations are shown in Table II. A strong metal-to-carbon bond is formed in both carbides. On the other hand, metal-to-metal bonding decreases on going from the metal to the carbide.²⁶ Hence, the great hardness of transition-metal carbides when compared to transition metals must be due to metal-to-carbon bonding, a fact which is consistent with the brittle nature of carbides. This result contradicts the suggestions of other authors²⁷ that metal-to-metal bonding increases on going from the metal to the carbide.

The explanation is as follows. In both cases carbon interacts with some of the metal-to-metal bonding orbitals. This results in a delocalization of the charge in these orbitals into metal-to-carbon bonds, and hence a loss of metal-to-metal bonding. Since metal-to-carbon bonding is stronger than metal-to-metal bonding this delocalization can be very strong, and later we will show that metal *e_g* orbitals in the solid-state carbide hardly participate in metal-to-metal bonding at all.

VI. Trigonal Prismatic vs. Octahedral

Trigonal-prismatic $M_6(CO)_n C$ clusters have four more electrons in bonding and nonbonding orbitals than do octahedral clusters. Hence, using our previous counting scheme, we would say they have 90 electrons. Once again we consider the cluster $Ru_6(CO)_{18}C$, since we can make use

(25) Heiniger, F.; Bucher, E.; Muller, J. *Phys. Kondens. Mater.* 1966, 5, 243.

(26) The comparison between metal and carbide M-M overlap populations using a constant M-M distance is consistent with the greater M-M distance in the carbide.

(27) (a) Reference 1a, p 146. (b) Samsonov, G. V.; Umanskiy, Ya. S. "Tverdye Soyedineniya Tugoplavkitch Metallov."; State Scientific and Technical Literature Publishing House: Moscow, 1957. (c) Kiessling, R. *Met. Rev.* 1957, 2, 77.

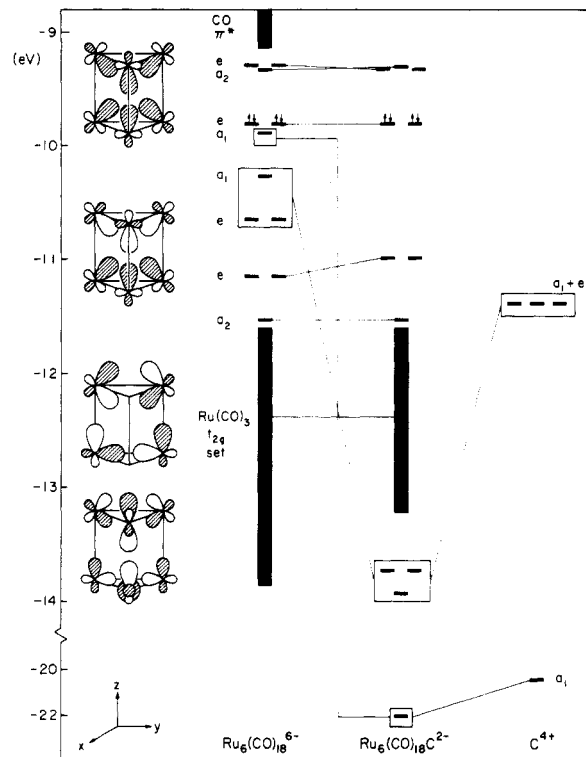


Figure 9. Interaction diagram for the formation of $Ru_6(CO)_{18}C$ from $Ru_6(CO)_{18}$ and C. The metal framework is trigonal prismatic. The boxed frontier orbitals drawn interact with carbon *s*, *p_z*, *p_y*, and *p_x* (top to bottom).

of the isolobal analogy between $Ru(CO)_3$ and BH. Since it is impossible to have more than three ruthenium orbitals participate in metal-to-metal bonding, the naked Ru_6 fragment gives the same result.

The interaction diagram, Figure 9, shows the details of metal-to-carbon bonding for our actual C_{3v} molecule (Appendix). The crucial point of the figure is that, before metal-to-carbon bonding is turned on, there are nine metal-to-metal bonding orbitals above the fragment t_{2g} set, instead of seven in the octahedron. The symmetries of these orbitals are easily obtained from group theory, when we divide the three frontier orbitals of $Ru(CO)_3$ into σ (parallel to the threefold axis) and π (perpendicular to the threefold axis). π_1 lies in a vertical mirror plane. Reduction from D_{3h} to C_{3v} removes the horizontal mirror plane ('').

$$\begin{array}{ll} \sigma: a_1', e' \text{ (bonding)} & a_2'', e'' \text{ (antibonding)} \\ \pi_1: a_1', a_2'' & e', e'' \\ \pi_2: a_1'', a_2' & e', e'' \end{array}$$

Once again, the major interaction of carbon *p* orbitals ($a_1 + e$) and *s* orbitals (a_1) is with occupied $Ru_6(CO)_{18}$ orbitals. Hence the electron count remains constant on forming the carbide; however, four out of nine frontier orbitals are pushed below the metal-to-metal bonding levels by bonding with carbon.

In the solid-state realm, although both the NaCl (octahedral) and WC (trigonal prismatic) structures are found for a range of electron counts, there is a definite dividing line (d^6), below which only the NaCl structure is found and above which the NaCl structure is rarely found (Table I). Once again, addition of electrons gives the trigonal-prismatic geometry. In order to best compare the WC to the NaCl structure, we used the same Mo parameters. As far as geometry is concerned, we had the choice of two extremes: (i) the same metal-to-carbon distance, which implies a shorter metal-to-metal distance or (ii) the same metal-to-metal distance, which implies a longer metal-to-carbon distance in WC. In practice, we used the experi-

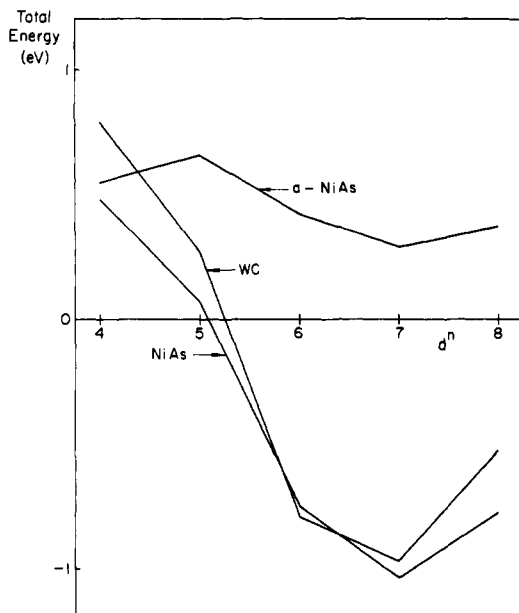


Figure 10. Total energy of the anti-NiAs, NiAs, and WC structures relative to the NaCl structure as zero. An energy below zero implies that the structure is favored relative to NaCl. An energy above zero implies that the NaCl structure is favored.

mental geometry for MoC (WC) and varied the MoC (NaCl) geometry to one of the above extremes.

The total energies (Figure 10) were obtained by keeping a constant metal-to-carbon distance. Total energies were obtained for the series of electron counts d^4 to d^8 and are plotted with the NaCl structure as zero energy. In other words, when WC lies above the base line, the NaCl structure is preferred; when WC lies below the base line, it is preferred to the NaCl structure. In perfect agreement with experiment, we see a shift in preference between d^5 (NbC) and d^6 (WC).

Actually, the WC structure differs from the NaCl structure in both the trigonal-prismatic metal framework and the trigonal-prismatic carbon framework. In order to determine the relative importance of carbon vs. metal, we calculated the intermediate structures NiAs and anti-NiAs. Again the metal-to-carbon distance was kept constant. Also, the metal framework was chosen to be uniform so that axial and equatorial metal-to-metal distances were equal. In the NiAs structure the metal framework is trigonal prismatic and the carbon framework octahedral, and it follows the WC structure in its energetics. The anti-NiAs structure, in which the metal framework is octahedral and the carbon framework trigonal prismatic, is parallel to the NaCl base line. Hence it is the metal framework that determines the shift in preference between d^5 and d^6 .

In Figures 2 and 3 we saw that metal-to-carbon bonding was constant over the energy range of interest; hence the difference between structures must lie in metal-metal bonding. In Figure 11 we have plotted on the left side the total metal-to-metal overlap populations, the integral of the COOP, for the series d^4 to d^{10} . Here, and in all instances where we discuss overlap populations, we have kept the average metal-to-metal distance constant between structures. For the octahedral metal framework (NaCl, anti-NiAs) the maximum in bonding occurs for electron count d^4 . Between d^4 and d^6 we fill antibonding orbitals. On the other hand, for a trigonal-prismatic metal framework (WC, NiAs) we fill bonding orbitals up to electron count d^6 . It is obvious why the shift in preference (Figure 10) occurs.

In order to better understand this difference, we need to break down the bonding, orbital by orbital. In fact, for

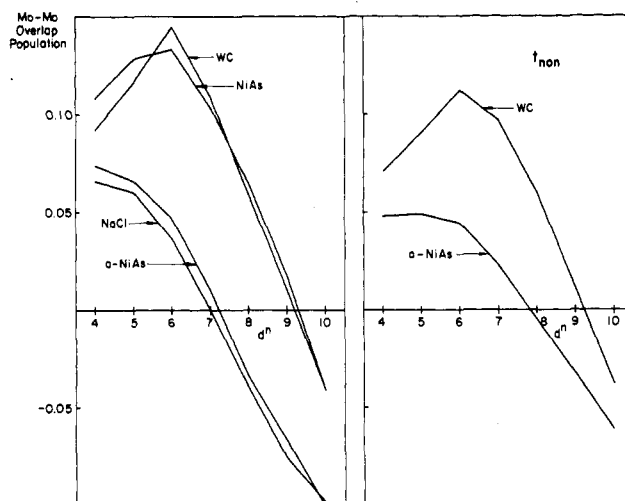


Figure 11. Overlap populations for the series of electron counts d^4 - d^{10} . The total overlap populations for four structures are on the left. The contribution from $(t_{\text{non}} - t_{\text{non}}) + (t_{\text{non}} - \text{sp})$, for two structures, is on the right.

reasons that will be obvious later, we have chosen to break the metal d orbitals into two groups, $t_{\text{non}} + e_{\text{anti}}$, according to the nature of their *metal-to-carbon* bonding character. A third group of metal orbitals, (sp), the s and p orbitals, are important contributors to the metal-to-metal overlap population (through hybridization) in spite of their relatively small occupation number. For trigonal-prismatic WC, it is natural to have the z axis parallel to the threefold axis of the prism. Figure 12 shows that the breakdown of metal-to-carbon bonding follows ligand field arguments; most bonding takes place with the d orbitals xz and yz (compare to Figure 7 and our earlier arguments). Hence, we divide the metal orbitals into three sets:

- (a) sp or $\{s, p_x, p_y, p_z\}$
- (b) t_{non} or $\{d_{xy}, d_{x^2-y^2}, d_{z^2}\}$
- (c) e_{anti} or $\{d_{xz}, d_{yz}\}$

It also seems logical to choose a coordinate system for the octahedron with z parallel to the S_6 axis.²⁸ This is not the natural coordinate system for fcc NaCl, but it is natural for anti-NiAs which has a hexagonal space group. Since Figures 10 and 11 show that anti-NiAs follows NaCl in every respect, it is reasonable to assume that by comparing anti-NiAs with WC we will get insight into the difference between the NaCl and WC structures.

At the end of our discussion of the octahedron, we implied that most metal-to-metal bonding in the carbide takes place in the t_{2g} set of d orbitals. A similar argument holds for the trigonal prism, where the metal-to-carbon nonbonding orbitals are now referred to as t_{non} . Confirmation is provided in Figure 11. Contributions to the overlap population from $(t_{\text{non}} - t_{\text{non}})$ and $(t_{\text{non}} - \text{sp})$ bonding on the right-hand side of the figure are plotted on the same scale as the total overlap populations on the left-hand side of the figure.

An implication of the above is that an anisotropic distribution of bonding within the parent metal can have drastic consequences for metal-to-metal bonding in the carbide. In Figure 13 we have plotted the overlap populations for the metal, having the same geometry as in the carbide but now minus carbon. The resulting molybdenum-to-molybdenum distance of 2.87 Å is larger than the equilibrium distance in the metal, 2.73 Å. Details of the

(28) In this geometry, the e_g set in octahedral MC_6 is actually a linear combination of (xz, yz) and $(xy, x^2 - y^2)$ with the former predominating. Hence, in neither the octahedron nor the trigonal prism is the t_{non} set completely nonbonding.

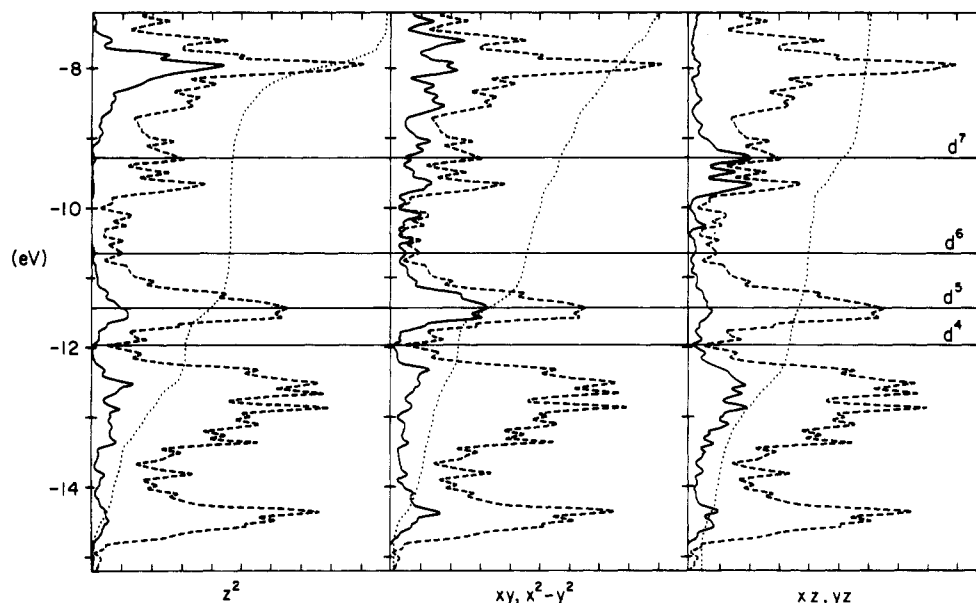


Figure 12. Projection (solid curves) of metal orbitals for MoC (WC). The total DOS (dashed) is provided for reference. The dotted curve is the integral of the projection on a scale of 0-100% full.

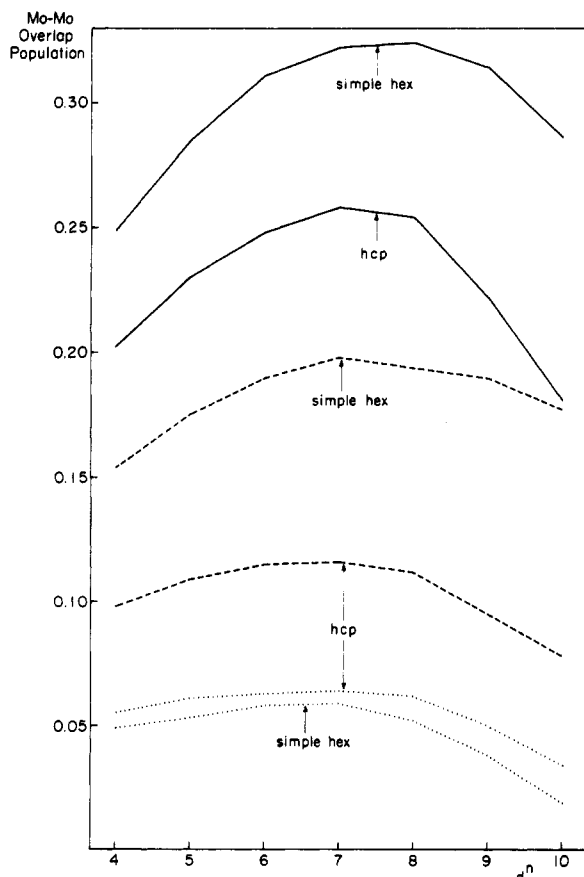


Figure 13. Overlap populations for the hexagonal close packed and simple hexagonal metals. Solid line: total. Dashed line: $(t_{\text{non}} - t_{\text{non}}) + (t_{\text{non}} - \text{sp})$. Dotted line: $(e_{\text{anti}} - e_{\text{anti}}) + (e_{\text{anti}} - \text{sp})$. "Non" and "anti" refer to potential metal-to-carbon bonding character on forming the corresponding carbides.

total overlap population are discussed later, for now we are interested in the division into $(t_{\text{non}} - t_{\text{non}}) + (t_{\text{non}} - \text{sp})$ bonding (dashed line) and $(e_{\text{anti}} - e_{\text{anti}}) + (e_{\text{anti}} - \text{sp})$ bonding (dotted line). Bonding in a close-packed metal is generally assumed to be isotropic. If bonding is equally divided among d orbitals the ratio $t_{\text{non}} - t_{\text{non}} : e_{\text{anti}} - e_{\text{anti}}$ is $3^2:2^2$, or 9:4. This is the approximate result for a hcp metal; however, for simple hexagonal metals bonding is weighted much more heavily into the t_{non} set. Not surprisingly, it is the non-close-packed structure that is more anisotropic.

Table III. Breakdown of Overlap Populations (Metal-Metal and Metal-Carbon) by Orbital for the Structures anti-NiAs and WC and Their Associated Parent Metal Lattices (Electron Count d^6)

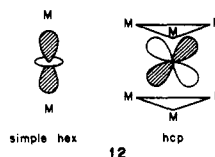
M-M bonding	equatorial		axial	
	hcp	simple hex	hcp	simple hex
$t_{\text{non}} - (t_{\text{non}} + \text{sp})$	0.174	0.189	0.057	0.198
$e_{\text{anti}} - (e_{\text{anti}} + \text{sp})$	0.027	0.042	0.099	0.102

M-M bonding	a-NiAs	WC	a-NiAs	WC
$t_{\text{non}} - (t_{\text{non}} + \text{sp})$	0.075	0.114	0.012	0.111
$e_{\text{anti}} - (e_{\text{anti}} + \text{sp})$	-0.003	0.003	0.012	0.027
sp-sp	-0.006	0.017	0.004	0.009

M-C bonding	a-NiAs	WC
p_x, p_y -carbon	0.047	0.061
$d_{x^2-y^2}, d_{xy}$ -carbon	0.037	0.027

The anisotropy can be understood by breaking metal-to-metal bonding into equatorial and axial components (Table III). By equatorial we mean the six neighbors in the xy plane of the metal; by axial we mean the two (WC) or six (anti-NiAs) neighbors resulting from stacking hexagonal nets along z . Differences in t_{non} bonding between the two metals (first two lines of Table III) are found for the axial bonds.

Structure 12 rationalizes this difference. In a simple



hexagonal lattice nearest neighbors lie along the z axis, and bonding takes place through $d_{z^2}(t_{\text{non}})$. In an hcp or fcc lattice the metal atom lies in a threefold hollow of the layers above and below, and bonding takes place through d_{xz} and d_{yz} (e_{anti}).

The result of anisotropy in bonding in the metal is that a much higher percentage of the metal-to-metal bonding orbitals remain occupied on formation of the WC structure than remain occupied on formation of the anti-NiAs carbide. This shows up in two ways. The peak metal-to-metal overlap population per bond is twice as large in WC as it

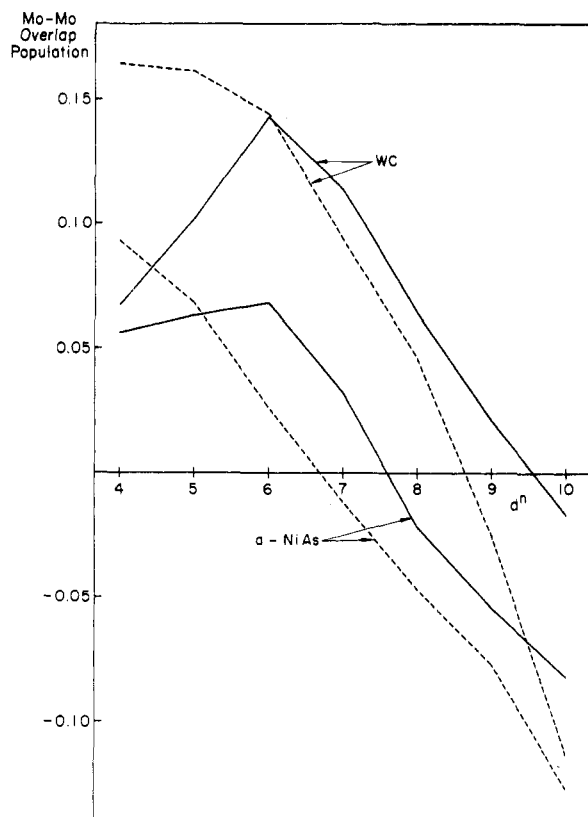


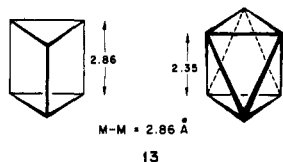
Figure 14. Overlap populations for the axial (dashed) and equatorial (solid) bonds in the WC and anti-NiAs structures.

is in anti-NiAs, easily overcoming an eight to twelve disadvantage in the number of nearest neighbors. The corresponding ratio in the metal is only five to four; this ratio cannot overcome the disadvantage in the number of nearest neighbors. This fact may explain why WC forms, although a simple hexagonal metal is unknown. It also may explain the experimental observation that certain measures of hardness, such as the Young's modulus,²⁹ are a maximum at the carbide of tungsten, d^6 , which naturally has the WC structure (here we are attributing differences in the mechanical properties of different carbides to metal-to-metal bonding).

Secondly, since there are more metal-to-metal bonding orbitals in WC, there is less of a shift in the peak overlap population to the left of the periodic table. This explains why the WC structure is preferred later in the periodic table.

So far we have only noted differences in axial bonding. However, Figure 14 shows that in the carbide there are also differences in equatorial metal-to-metal bonding between structures. The cause is no longer to be found in the metal; hence it must lie in differences in metal-to-carbon bonding.

The lowest two lines of Table III indicate the major differences between structures in metal-to-carbon bonding, divided orbital by orbital. In WC there is a greater con-



tribution from the set of p orbitals, x and y , and a smaller contribution from the set of d orbitals, xy and x^2-y^2 . The explanation is found in the dimensions of the MC_6 polyhedron. The height of this polyhedron is constrained to be the same as the height of the M_6C polyhedron. How-

ever, if metal-to-metal distances are the same, the trigonal-prismatic M_6C polyhedron must be taller (13). In other words we are talking about the c/a ratio. For WC, with a larger c/a ratio, carbon p interacts more with diffuse metal p orbitals and less with contracted metal d orbitals.

We recall that carbon interacts with bonding combinations of the metal orbitals. The effect on metal-to-metal bonding depends on whether the orbital is occupied or unoccupied in the metal. Occupied d orbitals lose electrons through delocalization onto carbon; unoccupied p orbitals gain electrons through delocalization from carbon. The net effect is that WC has more metal-to-metal bonding relative to anti-NiAs, both from the sp set and from the t_{non} set. This is shown in the middle three lines of Table III.

To summarize, for the solids, unlike the clusters, the preference for the hexagonal structure at higher electron counts is determined by the amount of electron transfer from metal-bonding orbitals to carbon. This amount is influenced both by anisotropy in metal-to-metal bonding in the metal as well as by differences in the orbital-by-orbital contribution to metal-to-carbon bonding. These differences in bonding are related to topological changes in the solid.

Interestingly, this change, with increasing electron count, between octahedral and trigonal-prismatic environments is not limited to the carbides. An analogous change occurs in the sulfides, except that the most common trigonal-prismatic structure is now NiAs (recall Figures 10 and 11). The dividing line, between ScS and TiS, is isoelectronic to the analogous dividing line in the carbides. The situation among phosphides is similar, though complicated by the appearance of other structures. For instance, the most common high-valence electron structure is MnP, which is closely related to NiAs.

We have not performed calculations specifically on the sulfides; however, Franzen et al. have used the LAPW method on the NaCl and WC forms of ZrS.³⁰ Some notable similarities between our two calculations are as follows: (i) An extra peak exists in the DOS for the WC structure below the d^6 Fermi level (Figure 12). Hence he would agree with the trend in total energy shown in Figure 10. (ii) Their conclusion that in plane (equatorial) M-M interactions stabilize the d^6 WC structure agrees with our discussion of how the c/a ratio affects equatorial M-M bonding.

VII. Other Solids

Classically, carbide structures have been discussed with use of an ionic model. Pauling radius ratios have been used to sort structures, and the results have been interpreted in terms of a steric effect. Two important conclusions that were first suggested by Hägg³¹ are as follows: (i) For monocarbides, the trigonal-prismatic structure is preferred for a smaller metal atom; the reason is that trigonal-prismatic coordination allows closer approach of the surrounding metal atoms (8). (ii) There is a magic number of 0.59 for the radius ratio of C/M.³² It is not possible to get a simple arrangement of metal atoms of the types hcp, fcc, or simple hexagonal if the radius ratio of C/M is greater than 0.59. Instead, the metal lattice distorts to one of the extremely complicated structures typical of the carbides of Cr to Ni. The explanation given is that for small enough metal atoms even a trigonal-prismatic arrangement of metal atoms around carbon does not allow

(30) Nguyen, T.-H.; Franzen, H.; Harmon, B. N. *J. Chem. Phys.* **1980**, *73*, 425-437.

(31) Hägg, G. *Z. Phys. Chem., Abt. B* **1931**, *B12*, 33-56.

(32) Clarke and Jack (Clarke, J.; Jack, K. H. *Chem. Ind. (London)* **1951**, 46, 1004) list a structure for Co_2C which appears to be an exception to this rule. It would be worth reexamining this structure.

Table IV. Extended Hückel Parameters

orbital	H_{ii}	exponents	orbital	H_{ii}	exponents
Fe 3d	-12.60	5.35 (0.5505) 2.00 (0.6260)	Mo 4d	-11.06	4.54 (0.5899) 1.90 (0.5899)
Fe 4s	-9.10	1.90	Mo 5s	-8.77	1.96
Fe 4p	-5.32	1.90	Mo 5p	-5.60	1.90
Ru 4d	-12.20	4.21 (0.5772) 1.95 (0.5692)	C 2s	-21.40	1.625
Ru 5s	-8.00	2.078	C 2p	-11.40	1.625
Ru 5p	-4.30	2.043	O 2s	-32.30	2.275
			O 2p	-14.80	2.275

enough metal-to-metal contact to stabilize one of these simple structures.

The purpose of this section is to apply bonding arguments developed in the previous section to understand some of this crystal chemistry. Where necessary we shall supplement our bonding arguments with arguments based on size.

Let us start with the monocarbides. We have already shown that for 10 or more valence electrons per formula unit the preferred structure is WC, not NaCl. The reason is that metal-to-metal bonding maximizes later in the transition-metal series for WC. However, we have not completely explained the preference for a NaCl structure at lower electron counts. For example, d^5 MoC contains more metal-to-metal bonding in the WC structure even when the differing number of nearest neighbors is taken into account (Figure 11).

Another unexplained point in Table I is the tendency for certain structures to prefer a NaCl structure, even though they may have 10 or more valence electrons. Most examples are borderline d^6 and can be explained by referring to their nonstoichiometry. CrN is an exception. CrN has an NaCl structure whereas MoN and WN have a WC structure. This is a size effect; however, the smaller metal atom takes on an octahedral geometry, contradicting the picture implied by point (i) above and by 8.

The explanation can be found by considering the MC_6 polyhedron and by using steric reasoning. Since carbon electrons are tied up in metal-to-carbon bonding, we can use VSEPR arguments.³³ These imply that the six metal-to-carbon bonds, and hence the six carbon atoms repel one another. Hence an octahedron, in which carbon atoms are furthest apart from one another, is favored (this is the classical argument used for ML_6 complexes). This additional effect causes the NaCl structure to be favored for d^5 metals, and only for d^6 , when much of the metal-to-metal bonding in the NaCl structure has been lost, is the WC structure favored in Figure 9. For the large C/M, or rather N/M, radius ratio found in CrN, nitrogen-to-nitrogen repulsion still favors the NaCl structure, even though CrN has 11 valence electrons and is isoelectronic with a d^7 carbide.

We are not the only authors to suggest a role for carbon-to-carbon repulsion. Parthe and Yvon⁹ used carbon-to-carbon repulsion to rationalize the structures of the subcarbides of early transition metals. One of their examples explains why the anti-NiAs structure is only found once, even though a similar hcp metal lattice is common for compounds of stoichiometry M_2C . In anti-NiAs the metal sublattice is different from the carbon sublattice. Hence, both sublattices cannot be uniform; i.e., all distances within the sublattice cannot be equal. In the preceding section, we showed that metal-to-metal bonding in anti-NiAs was isotropic. If we thus assume equal metal-to-metal distances, carbon-to-carbon contacts along the z

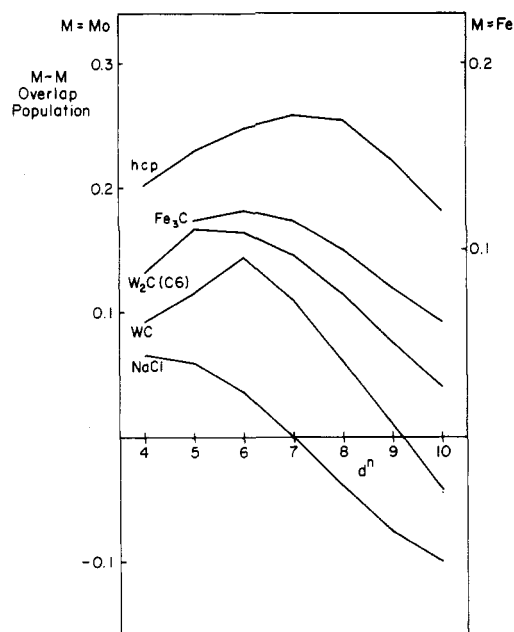


Figure 15. Overlap populations for an hcp metal and for four different carbides. In all cases except Fe_3C , Mo parameters and a Mo-Mo distance of 2.88 Å were used. Note the different scale for Fe.

axis must be shorter than metal-to-metal contacts along the z axis (see 13). For our chosen molybdenum-to-carbon distance, the carbon-to-carbon distance is 2.35 Å rather than 2.88 Å, which is what it would be if the carbon lattice was uniform. As a result, the energy of the anti-NiAs structure in Figure 10 is always somewhat higher than the energy of the NaCl structure. Some of this energy can be recouped by allowing a nonuniform metal sublattice, as is found experimentally.³⁴

On the other hand, in the anti-NiAs structure with a uniform metal lattice, the carbon-to-carbon distance along z is considerably longer than 2.88 Å. We might naively expect the NiAs structure to be favored over WC. What we have not considered is that we have lost ligand field energy by distorting a uniform MC_6 octahedron. In fact, Figure 10 shows NiAs to be competitive with WC, and our results do not suggest a reason for the absence of this structure.

In considering the subcarbides, we will first explain why monocarbides are not found late in the transition-metal series. Our explanation will be based on variation in bonding with electron count, not on size. We will also discuss the Fe_3C structure and some of the reasons for its being a preferred structure for late 3d transition metals.

In this section we performed calculations on two new structures, both of which were described earlier. One is the C6 or anti- CdI_2 structure adopted by low-temperature Ta_2C and W_2C . Here we used Mo parameters, and kept the molybdenum-to-molybdenum distance the same as for the other structures. The other is Fe_3C . Here we used Fe

(33) (a) Gillespie, R. J. "Molecular Geometry"; Van Nostrand-Rheinhold: London, 1972. (b) Gillespie, R. J.; Nyholm, R. S. Q. Rev., *Chem. Soc.* 1957, 11, 339.

(34) $(M-M)_{xy} = (N-N)_{xy} = 2.97$ Å. $(N-N)_z = 2.77$ Å. $(M-M)_z = 3.26$ Å. Reference 1a, p 93.

parameters and a geometry obtained from the crystal structure of $\text{Fe}_{2.7}\text{Mn}_{0.3}\text{C}$.^{12a} Because of differences in stoichiometry, we cannot compare the total energies of these two compounds. Instead, in Figure 15 we have plotted the total metal-to-metal overlap populations as a function of electron count for these two carbides, as well as the previously obtained results for the structures WC and NaCl and for an hcp metal. Overlap populations are, in general, smaller for 3d metals than for 4d or 5d metals; we used a different scale to plot the Fe-to-Fe overlap populations.

Let us first discuss the metal. There is a contribution to the overlap population from the d band which peaks at d^5 and is zero, actually negative, for a full d band. In addition, there is a contribution from the bottom of the s and p bands, and it is this contribution that ensures that d^{10} metals have a positive cohesive energy. In valence-bond language we could say that the metal was $d^9 s^1$, not d^{10} . Since the contribution from the s and p orbitals is bonding, it also shifts the maximal overlap population from d^5 to higher d electron counts. For normal metals at an equilibrium bond distance, this maximum is found for electron count d^6 ; melting temperatures of the transition metals also peak at this electron count.³⁵ In our case the metal-to-metal distance is typical of carbides and is larger than normally found in a metal. When the bond distance increases, the relative contribution of the diffuse s and p orbitals actually increases. Hence there are more bonding orbitals in the bottom of the band, and the maximal overlap population shifts to higher electron counts.

All of the other curves in Figure 15 are shifted down and to the left of that for the metal. From our studies on monocarbides, we know that this happens because of a transfer of electrons out of metal-to-metal bonding orbitals onto carbon. Not all orbitals are involved in this transfer, and hence there can be differences between different structures such as those between trigonal-prismatic WC and octahedral NaCl.

Apart from these differences due to the local geometry of the metal framework, there is also a general correlation between the relative amount of carbon and the loss of metal-to-metal bonding due to electron transfer. This is most easily seen when we compare the three cases in which the metal is close packed. In the sequence hcp, W_2C , and NaCl, the maximal overlap population shifts down and to the left of the figure. This explains why monocarbides of the late transition metals are rare and unstable.

We are now in a position to rationalize the Fe_3C structure. Since iron is one of the smallest transition metals, a trigonal-prismatic arrangement of metal atoms which allows closer metal-to-metal contact is preferred. Furthermore, a monocarbide of this late transition metal would be unstable due to the filling of antibonding orbitals. These two factors do not require a complicated lattice. Another possibility is ordered vacancies in a WC lattice, for example a $3^{1/2} \times 3^{1/2}$ covering of carbon for each layer of tungsten. On the other hand, the ratio carbon/iron is so low that each carbon atom can maximize bonding to iron atoms by including more iron atoms in its coordination sphere. Our calculations support this interpretation by indicating a sizable positive overlap population of 0.11 between carbon and two of the capping iron atoms in 7.

Here we see another advantage of the trigonal prism: the relatively large fourfold faces allow closer approach of a capping atom than do the threefold faces of an octahedron.

In any case, it is clear that $d^8 \text{Fe}_3\text{C}$ still retains a larger percentage of its maximal metal-to-metal overlap population than any other carbide in Figure 15.

Acknowledgment. We are grateful to Jane Jorgensen and Elizabeth Fields for the drawings and Sharon Drake for the typing. We would also like to acknowledge helpful discussions with other members of the group, especially Miklos Kertesz and Charles Wilker, and the useful comments of a reviewer. Our work was supported by the National Science Foundation through DMR Grant 7681083 to the Materials Science Center at Cornell and Grant CHE 7828048 and by the American Cyanamid Co.

Appendix

All extended Hückel parameters listed in Table IV are from previous work³⁶ except for the Ru H_{ii} . For both clusters, we used Ru-C (carbide) = 2.10 Å, Ru-CO = 2.00 Å, and C-O = 1.15 Å. The axis of the $\text{Ru}(\text{CO})_3$ fragment points toward the central carbon atom, with the angle OC-Ru-CO = 90°. The six fragments in the octahedral cluster were arranged so as to give a D_{3d} real geometry. We started with a D_{3h} geometry for the trigonal prism and then we rotated the three lower fragments by 60° each. Actual experimental geometries were used for Fe_3C (ref 12a) and $\text{MoC}(\text{WC})$: Mo-C = 2.1845 Å, (Mo-Mo)_z = 2.809 Å, (Mo-Mo)_{xy} = 2.898 Å. The same M-C distance, but a uniform M-M framework (M-M = 2.88 Å) were used for NiAs. For anti-NiAs and NbC, we used either (a) M-C = 2.1845 Å and M-M = 3.0894 Å or (b) M-C = 2.0335 Å and M-M = 2.8758 Å.

Special point sets for the solids were obtained by using the formulas of Monkhorst and Pack.³⁷ For each geometry, we used a large set of k points and a small set of k points. The large set was used for DOS curves and projections (including COOP). The small set was used for average energies and overlap populations in Figures 9-14. We verified convergence of these average properties by checking the small set against the large set for each geometry. In more detail these sets are NbC(fcc)-a 19 point set, and a 110 point set, using eq 3 of ref 37a with $q = 10$ and $q = 20$ and the procedure of Appendix A in this reference. WC, anti-NiAs, and NiAs all have hexagonal lattices and either D_{6h} or D_{3d} point symmetry. We used eq 1 of ref 37b for the xy plane. q_a was chosen to be 4 or 8. We used eq 2 of the same reference for the z axis. q_c was chosen to be 6 and 10 for WC and 3 and 6 for the other nonsymmorphic examples. Fe_3C (orthorhombic): the 8-point set was obtained by permuting $1/8$ and $3/8$ along three axes.

Registry No. $\text{Ru}_6(\text{CO})_{18}\text{C}^{2+}$, 89596-87-2; $\text{Ru}_6(\text{CO})_{18}^{2-}$, 62449-05-2; $\text{Ru}_6(\text{CO})_{18}^{6-}$, 89596-88-3; $\text{Ru}_6(\text{CO})_{18}\text{C}^{2-}$, 89596-89-4; C^{4+} , 16092-62-9; TiC, 12070-08-5; ZrC, 12070-14-3; HfC, 12069-85-1; VC, 12070-10-9; NbC, 12069-94-2; TaC, 12070-06-3; VN, 24646-85-3; MoC, 12011-97-1; WC, 12070-12-1; TaN, 12033-62-4; CrN, 24094-93-7; MoN, 12033-19-1; WN, 12058-38-7; Mo, 7439-98-7.

(36) (a) Summerville, R. H.; Hoffmann, R. *J. Am. Chem. Soc.* **1976**, *98*, 7240-7254. (b) Kubacek, P.; Hoffmann, R.; Havlas, C. *Organometallics* **1982**, *1*, 180-188. (c) Basch, H.; Gray, H. B. *Theor. Chim. Acta* **1966**, *4*, 367-376.

(37) (a) Monkhorst, H. J.; Pack, J. D. *Phys. Rev. B* **1976**, *13*, 5188-5192. (b) Pack, J. D.; Monkhorst, H. J. *Ibid.* **1977**, *16*, 1748-1749.

(35) Ashcroft, N. W.; Mermin, N. D. "Solid State Physics"; Holt, Rinehart and Winston: New York 1976, front cover.